Lidar-radar velocimetry using a pulse-to-pulse coherent rf-modulated Q-switched laser.

Marc Vallet, Jonathan Barreaux, Marco Romanelli, Grégoire Pillet, Jérémie Thévenin, Lihua Wang, Marc Brunel

Lidar-Radar velocimetry using a pulse-to-pulse coherent RF-modulated Q-switched laser

M. Vallet,[1*] J. Barreaux,[1§] M. Romanelli,[1] G. Pillet,[2] J. Thévenin,[1] L. Wang,[1] and M. Brunel[1]

[1]Institut de Physique de Rennes, Université de Rennes 1 – CNRS UMR 6251, Campus de Beaulieu, 35042 Rennes Cedex, France

[2]Thales Research and Technology, Campus Polytechnique, 1 Av. Augustin Fresnel, 91767 Palaiseau Cedex, France

[*]Corresponding author: marc.vallet@univ-rennes1.fr

Abstract: An RF-modulated pulse train from a passively *Q*-switched Nd:YAG laser has been generated using an extra-cavity acousto-optic modulator. The RF modulation reproduces the spectral quality of the local oscillator. It leads to a high pulse-to-pulse phase coherence, i.e., phase memory over thousands of pulses. The potentialities of this transmitter for Lidar-Radar are demonstrated by performing Doppler velocimetry on indoor moving targets. The experimental results are in good agreement with a model based on elementary signal processing theory. In particular, we show experimentally and theoretically that Lidar-Radar is a promising technique that allows discriminating between translation and rotation movements. Being independent of the laser internal dynamics, this scheme can be applied to any *Q*-switched laser.

OCIS codes: 140.3540, 280.3340, 280.3640

1. INTRODUCTION

Lidar-Radar is a powerful technique for applications involving remote sensing. The method is based on the use of an optically-carried radiofrequency (RF) signal in order to benefit from both the directivity of the optical beam (Lidar), and the accuracy of RF signal processing (Radar). In 1980, Eberhard and Schotland demonstrated wind velocity measurement using Doppler-shifted backscattering of dual-frequency laser beams on aerosols [1]. More recently, RF-modulated optical beams were proposed for the detection of underwater objects [2,3], leading to the development of 3D imagers [4]. At the same time, architectures based on dual-frequency sources were shown to provide accurate range and velocity measurements of moving targets in air, at short and long distances [5,6]. For long range detection, pulsed operation is required because the maximum range is proportional to the square of the retro-reflected power [5]. Moreover, to achieve high resolution, pulse-to-pulse coherence of the RF has to be preserved. Several kinds of transmitters fulfilling both pulsed operation and RF-coherence have been tested, based on i) external amplitude modulation [2], ii) phase-locked dual-seed pulsed laser [7], iii) cw dual-frequency lasers [8] injecting pulsed amplifiers [9], iv) pulsed dual-frequency lasers with frequency-shifted feedback [10]. Here, we propose to build a pulsed transmitter based on an external frequency-shifter and an original recombination technique. We apply this transmitter to velocity measurements on indoor targets in order to explore further potentialities of Lidar-Radar. Indeed, while radar imaging of moving targets are able to analyze different kinds of movements, such as vibration, rotation and translation, Lidar-Radar has been tested up to now for measuring the speed of target in translation only [6,9].

The aim of this paper is to show that a coherent pulse-to-pulse RF-modulated *Q*-switched laser is a convenient transmitter for Lidar-Radar and to study the Lidar-Radar response to rotation

and translation of the target. In Section 2, we detail the characteristics of the source based on a diode-pumped passively *Q*-switched Nd:YAG laser. The temporal and spectral characteristics of the emitted pulse train are reported and compared to the simulations derived from a rate-equation model. Section 3 presents an experimental demonstration of Doppler velocity measurement on indoor moving targets. The responses to linear and rotational motion of the target are presented separately in two subsections. Finally, Section 4 is devoted to the conclusion, where future improvements and possibilities are discussed.

2. RF-MODULATED LASER

The laser used in our experiments is schematized on Fig. 1. It consists in a diode-pumped passively *Q*-switched Nd:YAG laser (PQSL). The L = 95mm-long laser cavity is made of a high-reflection plane mirror M_1 coated on the 5mm-long Nd:YAG crystal and of a concave mirror M_2 (radius of curvature 100 mm; transmission T_2 of 1% at λ = 1064 nm). This leads to a free spectral range of the cavity equal to $c/2L$ = 1.58 GHz. The laser is passively *Q*-switched by an intracavity [100]-cut Cr:YAG saturable absorber crystal. The output laser pulses are typical of a Nd:YAG lasers *Q*-switched by a Cr:YAG crystal. When pumped at 808 nm with a pump power of 0.7 W, the laser emits a stable pulse train, in a single longitudinal mode, with a repetition rate of $1/T_{rep}$ = 3.5 kHz. The pulse width T_{pulse} and mean power P_L are respectively equal to 85 ns (FWHM) and 6.5 mW. The laser output beam of optical frequency ν is sent through an acousto-optic Bragg cell AO driven by a stable RF local oscillator LO (LO frequency f_{AO} = 88 MHz, LO power = 24 dBm). The frequency-shifted wave in the first diffraction order, with associated mean power P_1, is sent backwards the laser by means of the mirror M_3. The frequency of the beam sent back to the laser is hence equal to $\nu + 2f_{AO}$. It is then reflected by the cavity output mirror M_2 and it superposes to the laser output beam. Notice that, as $2f_{AO}$ is very different from the free spectral

range, the frequency-shifted beam is not expected to re-enter the laser cavity. This hypothesis is confirmed by the results presented in the following. The path from M_2 to M_3 is equal to 90 cm, corresponding to a round-trip time of 6 ns. The diffraction efficiency of the Bragg cell, defined as $\eta = P_1/P_L$, is here equal to 24%. Finally, the beam in the zero diffraction order provides the useful output signal. It corresponds to the coherent superposition of the laser output and of the frequency-shifted beam. Fig. 2(a) reports the experimental pulsed output versus time, with and without feedback. When the feedback is on, the beat note between the two optical frequencies ν and $\nu + 2f_{AO}$ clearly appears in the pulse envelope. Furthermore, the feedback beam does not modify the characteristics inherent to the *Q*-switched regime, as both pulse shape and duration are identical with and without feedback. From the inset of Fig. 2(a), the modulation depth of the beating frequency is estimated to be equal to $m = 42\%$. It is worthwhile to note that higher diffraction efficiency could lead to a larger value for m, but at the expense of reduced useful power in diffraction order 0. There is thus a trade-off between power and modulation depth.

In order to predict the behavior of the Nd:YAG laser, we model its dynamics using a usual set of rate equations [11]

$$\frac{dE_i}{dt} = \left(-\Gamma + \kappa n - a\right) E_i / 2 , \tag{1a}$$

$$\frac{dn}{dt} = \gamma_{//} \left(\left(a_0 + \Gamma\right) \rho / \kappa - n \right) - \xi \left|E_i\right|^2 n , \tag{1b}$$

$$\frac{da}{dt} = \gamma_a \left(a_0 - a\right) - \mu \left|E_i\right|^2 a , \tag{1c}$$

where E_i corresponds to the intracavity field, and n and a are the population inversion and saturable absorption loss coefficient, respectively. Note that, as the frequency-shifted optical field is supposed to be non-resonant, no feedback-dependent term has to be included in Eq. (1a). In the set of Eqs. (1), $\Gamma = -c/2L \times \ln(R_1 R_2 (1-\delta)^2)$ is the intensity loss coefficient, where $\delta = 0.005$ is the

single-pass loss coefficient. With the experimental parameters given before, it leads to $\Gamma = 3.17\ 10^7\ s^{-1}$. κ and ξ are the Nd^{3+} ion-field coupling coefficients. Using a proper normalization of E_i and n, one can take $\kappa = \xi = 1$. The relative excitation ρ was measured to be equal to 1.35. $\gamma_{//} = 4.35\ 10^3\ s^{-1}$ and $\gamma_a = 2.5\ 10^5\ s^{-1}$ are the relaxation rates of n and a, respectively. μ stands for the Cr^{4+} ion-field coupling in the absorber. μ depends of the relative laser mode size in the active medium and in the absorber [12]. It is thus the only adjustable parameter of the set of Eqs. (1) and was set to 2.85. $E_i(t)$ is calculated by a numerical integration of Eqs. (1a)-(1c). The output field $E_{out}(t)$ at mirror M_2 (see Fig. 1) can then be deduced from $E_i(t)$ using

$$E_{out}(t) = \sqrt{T_2}\ E_i(t) + \eta\sqrt{1-T_2}\ E_{out}(t-\tau)\ e^{4\pi j f_{AO} t} \quad . \tag{2}$$

At first order, Eq. (2) yields the following expression for the output power

$$P_{out}(t) \propto \left| E_i(t) + \eta\ E_i(t-\tau)\ e^{4\pi j f_{AO} t} \right|^2 . \tag{3}$$

Figure 2(b) reports the calculated output power evolution given by Eq. (3) for the two cases $\eta = 0.24$ and $\eta = 0$, i.e., when feedback is on and off. The agreement with the corresponding experimental pulses of Fig. 2(a) validates the assumptions underlying the model. In particular, it demonstrates that the non-resonant frequency-shifted field does not contribute to the intracavity field, and that the modulation depth only depends on the diffraction efficiency. Finally, we have also numerically checked that taking delays as long as the third of T_{pulse}, that is 25 ns, does not change the modulation depth at first order. By considering that $\tau \cong 0$, the output power P_{out} can thus be expressed analytically as a T_{rep}-periodic pulse train modulated by a beat note at frequency $2\ f_{AO}$, that is

$$P_{out}(t) = \left[1 + m\ \cos(4\pi f_{AO} t + \varphi_0(t))\right] \left[A(t) \otimes \Delta_{T_{rep}}(t) \right] \quad . \tag{4}$$

Here, $A(t)$ represents the pulse power envelope and $\Delta_T(t)$ is the Dirac comb of period T. $\varphi_0(t)$ the phase of the RF signal driving the Bragg cell. m is the modulation depth, equal to $2\eta/(1+\eta^2)$. A diffraction efficiency of 24% leads to m = 46% in good agreement with the experimental value. We point out that, although the modulation depth may seem low compared to the 100% available with other pulsed Lidar-Radar architecture [10], it is large enough to realize efficient velocity measurements on moving targets, as will be shown in the next section.

We now want to study theoretically and experimentally the spectral purity of the RF modulation by considering the power spectral density S_P of the pulse train. The Fourier transform of Eq. (4) yields

$$\tilde{P}_{\text{out}}(f) = \frac{1}{T_{\text{rep}}} \sum_n \tilde{A}\left(n/T_{\text{rep}}\right) \left\{ \delta(f - n/T_{\text{rep}}) + \frac{m}{2} \left[F_{\varphi_0}(f - 2f_{\text{AO}} - n/T_{\text{rep}}) + F_{-\varphi_0}(f + 2f_{\text{AO}} - n/T_{\text{rep}}) \right] \right\}. \tag{5}$$

$\tilde{A}$ is the Fourier transform of A, δ the Dirac delta-function and F_{φ_0} is the Fourier transform of $e^{j\varphi_0(t)}$. Assuming that the coherence time of φ_0(t) is long compared to T_{rep}, F_{φ_0} can be approximated by a delta function. One gets

$$\left|\tilde{P}_{\text{out}}(f)\right|^2 = \frac{1}{T_{\text{rep}}^2} \sum_n \left|\tilde{A}\left(n/T_{\text{rep}}\right)\right|^2 \left\{ \delta(f - n/T_{\text{rep}}) + \frac{m^2}{4} \delta(f - 2f_{\text{AO}} - n/T_{\text{rep}}) + \frac{m^2}{4} \delta(f + 2f_{\text{AO}} - n/T_{\text{rep}}) \right\}. \tag{6}$$

In writing Eq. (6), we have used the fact that the spectral width of Ã is of the order of $1/T_{\text{pulse}}$, thus smaller than 2 f_{AO}. This ensures that the cross terms vanish.

The first term in Eq. (6) corresponds to the low-frequency components inherent to pulsed regimes, while the second and third terms, around $2f_{\text{AO}}$ and $-2f_{\text{AO}}$ respectively, are due to the

beating between the laser and the frequency-shifted beam. For a restricted domain of frequency around $2\,f_{AO}$, S_p thus writes

$$S_p(f) \propto \frac{m^2}{T_{rep}^2} \sum_n \left|\tilde{A}(n/T_{rep})\right|^2 \delta(f - 2f_{AO} - n/T_{rep}). \quad (7)$$

Eq.(7) shows that S_p consists in a $1/T_{rep}$-periodic Dirac comb within an envelope given by $\tilde{A}$. The experimental spectral density of the beat note is reported on Fig. 3. Over a 500 MHz span frequency window (Fig. 3(a)), we observe a strong peak at $2f_{AO}$ = 176 MHz. The beat note has a 12 MHz full width at half maximum (FWHM), in agreement with the 85 ns pulse duration. The weak peak at $4f_{AO}$ is due to the beam which propagates four times in the Bragg cell and which has been disregarded in the former analysis at first order. Fig. 3(b) corresponds to a 30-kHz frequency span. The spectrum now consists in a 3.5 kHz periodic comb, as expected from Eq. (7). Further reduction in the frequency span permits to measure the linewidth of the central peak at $f = 2\,f_{AO}$. It is lower than 1 Hz (instrument limited) in agreement with a separate measurement of the LO linewidth. This linewidth shows that the pulse-to-pulse phase coherence of the RF modulation is sustained over more than 1 s, i.e. 3500 pulses.

Our method can be applied to any type of *Q*-switched laser for generating highly coherent RF-modulated pulsed beams, as it does not rely on the laser dynamics. In particular, it could be used to modulate the output power of high-power multimode *Q*-switched lasers. Indeed, in such lasers, longitudinal modes do not present pulse-to-pulse phase coherence. Additional interference terms (due to beatings between longitudinal modes) in Eq.(3) will have a random phase. As the coherence of the RF modulation allows measurements over many pulses, the interference terms will vanish and the contributions of the different longitudinal modes in Eq.(3) will add separately. Moreover, analysis of the power spectrum around $2f_{AO}$ would contribute to filter residual components due to intermodal beatnotes.

In order to test the potentialities of our source for Lidar-Radar, we have realized three experiments. They correspond to the detection of the velocity of a target placed either on a translating or on rotating stages. In all the following, the coherence of the pulse train permits to measure and process signals over a typical 1s integration time.

3. VELOCITY MEASUREMENT

Lidar-Radar architecture based on modulated pulsed trains benefit from both time-of-flight and Doppler phase shift detection to get the position and velocity of a target. Here, we focus on the velocity by reporting measurements on indoor targets with controlled movements.

A. Linear motion

The first experiment is described on Fig. 4. The emitted pulse train from the RF-modulated passively *Q*-switched laser is collimated and directed through a polarization beam splitter PBS followed by a quarter wave plate onto a target located at about two meters from PBS. The rays impinging on the target are thus circularly polarized. The target consists of a $4\,\mathrm{cm}^2$ retro-reflective tap mounted on a 2.5-meter long driving belt. The target can move towards or backwards the laser at a speed v adjustable from 0 up to $3.3\,\mathrm{m.s}^{-1}$, and it interacts with the incident beam over a distance L equal to about one meter. Assuming a pure linear motion for the target, the Doppler shift f_D on the RF modulation simply writes $4(v/c)\,f_{AO}$. To measure f_D, the backscattered optical power P_R reflected by PBS is collected with a 1-inch diameter lens and detected by a photodiode. Then, the electrical signal is amplified (40 dB gain) and sent onto a spectrum analyzer in order to calculate its power spectral density (PSD). The signal processing is

thus simply a Fourier transform, with a resolution bandwidth (RBW) here equal to 1 Hz. The Lidar-Radar measurement is performed on the central spectral component S_R around 2 f_{AO} of the PSD of $P_R(t)$, as shown in Fig. (5). This component is frequency-shifted when v varies, as evidenced by the experimental PSD. Indeed, a target velocity v = 1.8 m.s^{-1} leads to a frequency-shift of 2 Hz for S_R, in agreement with the theoretical value of the Doppler shift f_D = 2.1 Hz. Moreover, it has opposite sign for motions of the target backwards or towards the laser, as expected. Concerning the resolution associated to the measurement of the target velocity, one can suppose that it is only governed by RBW, i.e., instrument-limited. This yields a resolution equal to (c/4f_{AO})×RBW = 80 cm. s^{-1}. In addition, we observe that the width of the peak increases with respect to v (note the difference between v = 0 and v = 1.8 m.s^{-1} in Fig. 5). This is due to the finite interaction time $\tau = L/v$ of the light beam with the target inherent to our indoor measurement. Indeed, if one models the interaction time window by a rectangular function Π_τ, defined as $\Pi_\tau(t) = \{ 1 \ if \ |t| \le \tau/2 \ ; 0 \ if \ |t| > \tau/2 \}$, then the measured profile S_R is approximated by the following convolution product

$$S_R \propto \left|\tilde{\Pi}_{1/\tau}(f)\right|^2 \otimes \delta\left(f - 2f_{AO} - f_D\right), \tag{8}$$

where $\tilde{\Pi}_{1/\tau}$ is the Fourier-transform of Π_τ. The theoretical width of the peak is thus of the order of $1/\tau$. For instance, since L = 1m, it is equal to 1.8 Hz when v = 1.8 m.s^{-1}, in good agreement with the experimental 1.7 Hz obtained from the spectra of Fig. (5). Finally, Doppler shift measurements at different values of v have been reported on Fig. 6. The experimental dots are perfectly aligned, which confirms the reliability of the Lidar-Radar method.

B. Rotating diffusing panel

In a second set of experiments, we have investigated the response associated to a rotating target. The experimental setup is identical to the one sketched on Fig. 4 except that the target now consists of retro-reflecting tape on the face of a disk attached to a DC motor with an angular velocity $2\pi/T = 850$ rad.s^{-1}, as schematized on Fig. 7(a). The target inclination angle θ and the distance R between the laser spot and the axis of rotation are set at 45° and 4 cm, respectively. The component v along the optical axis of the laser spot velocity v_{spot} is thus equal to $2\pi R/T \times \cos\theta = 24$ m.s^{-1}, leading to an expected Lidar-Radar Doppler shift $f_D = 28$ Hz. However, we did not observe any frequency shift on the PSD associated to the backscattered light, as the central spectral component S_R stayed exactly at $2 f_{AO}$, independently of v.

Curiously, the Lidar-Radar measurement seems to be insensitive to the rotation of the target, although it is well-known that rotating diffusing panels similar to the one of Fig. 7(a) shift the frequency of a laser beam [13,14]. One can therefore wonder why, since each optical frequency is Doppler-shifted, their difference is independent of the target speed. To answer this question, we first checked the optical Doppler shift using a standard coherent detection scheme, i.e. by mixing a reference beam to the beam backscattered from the target. We measured a frequency shift equal to $2v/\lambda$, as expected. Secondly, we calculated the PSD of the backscattered power by using a linear model, as is now discussed.

Let us consider a normalized continuous optical power P_i impinging on the target that is modulated at $2 f_{AO}$. It writes, in complex notation, $P_i(t) = \exp(j\phi(t))$, where $\phi(t) = 4\pi f_{AO} \times t$ is the phase associated to the RF modulation. The target is supposed to be made of q small diffusers equally distributed along the closed trajectory. An estimation of q is made by supposing that q is

equal to 2πR divided by the laser spot diameter on the target. Each elementary diffuser reflects the laser beam during a time T/q. Here, one finds $T/q \cong 35$ µs. The sum of the optical powers backscattered by the q diffusers can be expressed as a product of three terms

$$P_{\mathrm{R}}(t) = \sum_{p=0}^{q-1} \left\{ \left(\Pi_{T/q} \otimes \Delta_T \right)(t - pT/q) \times \exp\left(j\varphi\left(t + D\left((t - pT/q)[T] \right) \right) \right) \times \exp\left(j\varphi_{p,0} \right) \right\} \quad , (9)$$

where $D(t)$ is equal to $2\mathrm{v}/\mathrm{c} \times t$. $[T]$ stands for the T-modulo operation, i.e., $(t - pT/q)[T]$ is equal to the remainder of the Euclidian division of expression in brackets $t - pT/q$ by T. $\varphi_{\mathrm{p},0}$ corresponds to the phase-shift induced by the p^{th}-diffuser. The first term in the sum corresponds to the T-periodic modulation of the reflected power. The second term governs the RF phase. The function $D(t)$ gives a time lag leading to the Doppler phase shift. Evaluating the time lag modulo T is mandatory in order to take into account the fact that the target rotates, that is, the diffusers come back to the same position every T. In the last term, $\varphi_{\mathrm{p},0}$ is a phase shift at $t = 0$ induced on the RF modulation by the p^{th}-diffuser. As the synthetic wavelength $\Lambda = \mathrm{c}/(2f_{\mathrm{AO}}) = 1.5$ m is very large compared to the difference of successive positions of the diffusers when they pass into the laser spot, $\varphi_{\mathrm{p},0}$ can be assumed to be constant. In other words, the random character of the target, which leads to speckle at optical wavelengths, is irrelevant at the synthetic wavelength. Without loss of generality, we choose $\varphi_{\mathrm{p},0} = 0$. The PSD of the detected signal can then be calculated using Eq. (9), as detailed in Appendix A. It writes

$$S_{\mathrm{R}}(f) = \sum_n \frac{q^2}{T^2} \left| \tilde{\Pi}_{q/T}(nq/T - f_D) \right|^2 \times \delta(f - 2f_{\mathrm{AO}} - n/T) . \qquad (10)$$

It consists of a Dirac comb centered at $2f_{\mathrm{AO}}$ of periodicity $1/T$. The amplitude of each frequency component of the comb is given by the function $\left|\tilde{\Pi}_{q/T}\right|^2$ taken at $nq/T - f_{\mathrm{D}}$. Then, since the width of $\left|\tilde{\Pi}_{q/T}\right|^2$ is of the order of q/T, the only peak with significant power corresponds to

$nq/T - f_D \approx 0$. Experimentally, the mean size of the laser spot on the target is small enough to assume that q/T is much larger than f_D. One must hence take $n = 0$ in Eq. (10). Using $\tilde{\Pi}_{q/T}(f_D) \cong \tilde{\Pi}_{q/T}(0) = T/q$, one has

$$S_R(f) = \frac{q^2}{T^2}\left|\tilde{\Pi}_{q/T}(f_D)\right|^2 \times \delta(f - 2f_{AO}) \cong \delta(f - 2f_{AO}). \quad (11)$$

This equation shows that the optically-carried RF is not Doppler-shifted by the rotation of the target, in agreement with our experimental observations. Besides, the former expression of the PSD around 2 f_{AO} remains valid when one takes into account the pulsed dynamics of the laser beam. A straightforward calculation shows that using expression (4) for $P_i(t)$ again leads to Eq. (11).

The preceding analysis is based on the assumption that the target is made of multiple diffusors and suggests that the Doppler response is jammed by the summation of the different contributions. A second experiment permits to give further insight on this effect.

C. Rotating corner cube

The rotating reflector is now a non-diffusing target. It is a corner cube mounted on a rotating arm, as shown in Fig. 7(b). We suppose a pure specular reflection on the corner cube and that the spatial quality of the beam is maintained. The rotation frequency is $1/T$ = 4.1 Hz. The distance R between the axis of rotation and the corner cube is equal to 19.5 cm, leading to a radial velocity v = 5.1 m.s^{-1}. At this speed, from the duration of the pulse train detected by the photodiode, we deduce that the corner cube reflects backwards the incident beam during a time $\tau \cong 13$ ms. Using the same notations as the ones of Eq. (8), the reflected power can be written

$$P_{\mathrm{R}}(t) = \left(\Pi_{\tau} \otimes \Delta_{T}\right)(t) \;\times\; \exp\left(j\varphi\left(t + D\left(t\left[T\right]\right)\right)\right). \tag{12}$$

The PSD of the collected reflected beam (see relation (A10) of Appendix A) is then given by

$$S_R(f) = \frac{1}{T^2}\sum_n \left|\tilde{\Pi}_{1/\tau}(n/T - f_D)\right|^2 \delta\left(f - 2f_{AO} - n/T\right). \tag{13}$$

As for Eq.(9), it consists in a Dirac comb centered at $2f_{\mathrm{AO}}$ of periodicity $1/T$. Here again, the spectral components are not Doppler-shifted, but each comb frequency has now an amplitude given by the function $\left|\tilde{\Pi}_{1/\tau}\right|^2$ taken at $n/T - f_{\mathrm{D}}$ instead of $nq/T - f_{\mathrm{D}}$. It means that many comb frequencies have non-vanishing amplitudes. Furthermore, the comb frequency that has the largest amplitude corresponds to $n/T - f_{\mathrm{D}} \approx 0$. Unlike the Lidar-Radar response of the rotating panel, in the case of the Lidar-Radar signal provided by only one diffusor, one can expect to measure the rotation-induced Doppler shift from the comb envelope shift, as long as it is not too small compared to the width of the envelope. This is confirmed by our experiment. Fig. (8) shows the experimental PSD of the reflected optical power. The frequencies associated to the comb are independent of the Doppler shift. The experimental envelope is fitted by a Gaussian function (dashed line in Fig. (8)). The fit yields a translation factor of 6.0 ± 0.4 Hz, in agreement with the expected value $f_{\mathrm{D}} = 4\mathrm{v}/c \times f_{\mathrm{AO}} = 5.9$ Hz. We also verified that the opposite sense of rotation yields an opposite Doppler shift.

From these two experiments on rotating targets of different nature, that is, one made of q elementary diffusors and one made of a perfect specular reflector, we find that the condition that has to be met to resolve without difficulty a small f_{D} associated to a rotation is that f_{D} be comparable with the inverse of the interaction time with the target. Or, in other words, the interaction length has to be comparable with $\Lambda/2$. We stress that this rule of thumb does not prevent from measuring shifts that are smaller than the interaction time, at the expense of a more

elaborate signal analysis. In the experiment with the rotating panel, the inverse of the interaction times is equal to q/T = 35 kHz, which is far greater than f_D. In the case of the corner cube, the inverse of the interaction time is equal to $1/\tau$ = 77 Hz. However, a Doppler shift of 6 Hz can still be detected from the data on Fig. (8) by fitting the signal envelope.

Finally, by using the same model as before, one can show that combined translation and rotation movement for the corner cube would result in a spectral density of the form (see appendix A)

$$S_R(f) = \frac{1}{T^2}\sum_n \left|\tilde{\Pi}_{1/\tau}(n/T - f_{DR})\right|^2 \delta\left(f - 2f_{AO} - f_{DT} - n/T\right), \tag{14}$$

where $f_{DT,DR} = 4v_{T,R}/c \times f_{AO}$ are the Doppler shifts associated to the linear velocity of translation v_T and to the radial velocity component v_R due to the rotation, respectively. We see that the comb is frequency-shifted by f_{DT} and that the envelope is shifted by f_{DR}. One can thus discriminate between rotation and translation. In the case of the diffusing panel, one would get

$$S_R(f) = \delta(f - 2f_{AO} - f_{DT}). \tag{15}$$

Again, the PSD frequency is only Doppler-shifted by the translation movement.

4. CONCLUSION

We have reported a simple method for generating a radio-frequency (RF) modulated optical pulse train and investigated its potentialities for Lidar-Radar. An experimental design, based on a passively *Q*-switched Nd:YAG laser and a feedback arm containing an acousto-optic modulator, was shown to provide a modulation depth of 41 % and a RF phase coherence over thousands of pulses. These results are well supported by a rate equation model. In order to test the potentialities of our Lidar-Radar transmitter, we performed Doppler velocimetry measurements.

The Doppler signature was obtained from the power spectral density (PSD) of the backscattered beam from indoor targets. The experimental results are in full agreement with the theoretical PSDs obtained from a simple analytical model. Importantly, we have demonstrated that, unlike coherent Lidars, the Lidar-Radar is not sensitive to rotation if the product of the Doppler shift by the interaction time is too small. In other words, the synthetic wavelength must be short enough to allow the detection of rotation movement. This is an interesting point because it shows that the Lidar-Radar can discriminate between pure translation and rotation.

Further investigations can now be performed. Full advantage of the pulsed operation could be taken by using matched filtering instead of single frequency detection [9,15]. The analysis described above has been done for a pure sinusoidal RF signal but it can be extended to other modulation formats, such as, for instance, RF frequency chirping. This study could also give clues to detect micro-Doppler signature, where vibrations and rotations have to be discriminated [16]. As the method can be used with virtually any *Q*-switched lasers, it could be applied with green lasers for underwater remote sensing where visible light is mandatory [4,17]. Our method could also be useful to build Lidar-Radar architecture with promising sources recently used in coherent Doppler lidar systems, such as mode-locked lasers [18] or compact fiber lasers [19].

ACKNOWLEDGMENTS

Partial support for this work was provided by the Contrat de Projet Etat-Région “PONANT”. We thank A. Carré and C. Hamel for technical assistance.

§ Now at Laser Physics and Nonlinear Optics, University of Twente, Postbus 217, 7500 AE Enschede, The Netherlands.

APPENDIX A

In this section, we derive the power spectral density S_R of the reflected optical power P_R for the rotating targets schematized on Fig. 7. We also discuss the case of a target movement composed of both translation and rotation.

1 Rotating diffusing panel

In the case of rotating diffusers (see Fig. 7(a)), the backscattered power $P_R(t)$ is given by Eq. (9) with $\phi(t) = 4\pi f_{AO} \times t$, $D(t) = 2v/c \times t$ and $\varphi_{p,0} \cong 0$. It yields

$$P_R(t) = \sum_{p=0}^{q-1} \left\{ \left(\Pi_{T/q} \otimes \Delta_T \right)(t - pT/q) \ \times \ \exp\left(4\pi j f_{A0} t + 2\pi j f_D \left((t - pT/q)[T] \right) \right) \right\}. \quad \text{(A1)}$$

From the identity

$$\exp\left(2\pi j f_D (t[T]) \right) = \left(\Pi_T(t) \exp\left(2\pi j f_D t \right) \right) \otimes \Delta_T(t), \quad \text{(A2)}$$

one gets

$$P_R(t) = e^{4\pi j f_{A0} t} \sum_{p=0}^{q-1} \left\{ \left(\Pi_{T/q}\left(t - pT/q \right) \Pi_T\left(t - pT/q \right) \exp\left(2\pi j f_D (t - pT/q) \right) \right) \otimes \Delta_T(t - pT/q) \right\}. \quad \text{(A3)}$$

That is

$$P_R(t) = e^{4\pi j f_{A0} t} \sum_{p=0}^{q-1} \left\{ \left(\Pi_{T/q}(t - pT/q) \exp\left(2\pi j f_D (t - pT/q) \right) \right) \otimes \Delta_T(t - pT/q) \right\}. \quad \text{(A4)}$$

The Fourier-transform of the received signal becomes

$$\tilde{P}_R(f) = \delta\left(f - 2 f_{AO} \right) \otimes \left(\frac{1}{T} \sum_{p=0}^{q-1} e^{2\pi j (pT/q) f} \ \tilde{\Pi}_{q/T}(f - f_D) . \Delta_{1/T}(f) \right), \quad \text{(A5)}$$

which can be written as

$$\tilde{P}_R(f) = \delta\left(f - 2f_{AO}\right) \otimes \left(\frac{1}{T} \sum_{p=0}^{q-1} e^{2\pi j\, pn/q} \sum_n \tilde{\Pi}_{qT}(n/T - f_D)\, \delta\left(f - n/T\right) \right), \tag{A6}$$

to give

$$\tilde{P}_R(f) = \frac{1}{T} \sum_n \left\{ \left(\sum_{p=0}^{q-1} e^{2\pi j\, pn/q} \right) \tilde{\Pi}_{q/T}(n/T - f_D)\, \delta\left(f - 2f_{AO} - n/T\right) \right\}. \tag{A7}$$

Finally, using the identity $\sum_{p=0}^{q-1} e^{2\pi j\, pn/q} = \left\{ q \ \textit{for}\ n[q] = 0 \ ;\ 0 \ \textit{for}\ n[q] \neq 0 \right\}$, one gets

$$\tilde{P}_R(f) = \frac{q}{T} \sum_n \left\{ \tilde{\Pi}_{q/T}(n/T - f_D)\, \delta\left(f - 2f_{AO} - n/T\right) \right\}. \tag{A8}$$

It leads to Eq. (10) of Subsection (3B).

2 Rotating corner cube

In the case of a target consisting in one rotating corner cube, as schematized on Fig. 7(b), the reflected power $P_R(t)$ can be obtained from Eq. (A3)

$$P_R(t) = e^{4\pi j f_{A0} t} \left(\left(\Pi_\tau(t) \exp\left(2\pi j f_D t\right) \right) \otimes \Delta_T(t) \right) \tag{A9}$$

where τ is the duration of reflection of the corner cube. It leads to

$$\tilde{P}_R(f) = \frac{1}{T} \sum_n \left\{ \tilde{\Pi}_{1/\tau}\left(n/T - f_D\right) \delta\left(f - 2f_{AO} - n/T\right) \right\}. \tag{A10}$$

The PSD associated to P_R is then deduced from (A10), leading to Eq. (13) of Subsection (3C).

3 Both translation and rotation

We now consider a diffusing panel having a movement of linear translation and of rotation. The translation velocity is written v_L and the radial velocity component due to rotation is written v_R

From Eq.(8), one gets

$$P_{\mathrm{R}}(t)=\sum_{p=0}^{q-1}\left\{\left(\Pi_{T/q}\otimes\Delta_{T}\right)(t-pT/q)\ \times\ \exp\left(\ j\varphi\left(t+D_{T}(t-pT/q)+D_{R}\left((t-pT/q)\left[T\right]\right)\right)\right)\ \right\}$$

(A11)

with $D_{L,R}(t)=2\frac{\mathrm{v}_{L,R}}{c}t$. Using $f_{DT,DR}=4\frac{\mathrm{v}_{T,R}}{c}\,f_{AO}$ and (A2), it gives

$$P_{\mathrm{R}}(t)=e^{2\pi j(2f_{\mathrm{A0}}+f_{DT})t}\sum_{p=0}^{q-1}\left\{\left(\Pi_{T/q}(t-pT/q)\exp\left(2\pi jf_{\mathrm{DR}}(t-pT/q)\right)\right)\otimes\Delta_{T}(t-pT/q)\right\}. \quad \text{(A12)}$$

From the set of Eq.(A3-A7), a straightforward calculation yields to the expression (15) for the PSD $S_{\mathrm{R}}(f)$.

In the case of the corner cube, the reflected power writes

$$P_{\mathrm{R}}(t)=\left(\Pi_{\tau}\otimes\Delta_{T}\right)(t)\ \times\ \exp\left(\ j\varphi\left(t+D_{T}(t)+D_{R}\left(t\left[T\right]\right)\right)\right), \quad \text{(A13)}$$

That is, using (A2)

$$P_{R}(t)=e^{2\pi j(2f_{AO}+f_{DT})t}\left(\Pi_{\tau}(t)\exp(2\pi jf_{DR}t[T])\right)\otimes\Delta_{T}(t)\ . \quad \text{(A14)}$$

With the help of Eqs (A3-A6), one gets expression (14) for the the PSD $S_{\mathrm{R}}(f)$.

FIGURE CAPTIONS

Fig. 1: Experimental setup of the transmitter. PQSL: passively *Q*-switched Nd:YAG laser. $M_{1,2}$: cavity mirrors. LD: laser diode. AO: acousto-optic frequency shifter driven by a local oscillator LO. M_3: feedback mirror. L: matching lens.

Fig. 2: (a) Experimental output pulse power versus time. Inset: 25 ns time window centered at the pulse peak power. (b) Output pulse obtained from a rate equation model.

Fig. 3: Electrical spectral analysis of the output power. (a) Span 500 MHz; resolution bandwidth (RBW) 30 kHz. (b) Span 30 kHz; RBW 30 Hz; the horizontal axis corresponds to the spectrum analyzer floor (-100 dBm).

Fig. 4: Schematic of the experimental setup for measuring the linear velocity v of an indoor target. PBS: polarization beamsplitter. QWP: quarter wave plate.

Fig. 5: Spectral analysis of the optical power backscattered by a target having a linear motion with velocity v. As schematized, the power spectral density is shown around $2\,f_{AO}$. Left peak: $v = -1.8$ m.s^{-1}. Central peak: $v = 0$ m.s^{-1}. Right peak: $v = 1.8$ m. s^{-1}. Span: 50 Hz. RBW: 1 Hz.

Fig. 6: Experimental Doppler shift f_D versus target velocity v.

Fig. 7: Schematic of the experimental setups to study rotation of indoor targets. (a) Rotating diffusing panel. (b) Rotating corner cube. See text for details.

Fig. 8: Experimental PSD around $2f_{AO}$ of the signal reflected by a rotating corner cube. Span 100 Hz; RBW 1 Hz. Dashed line: Gaussian fit of the envelope.

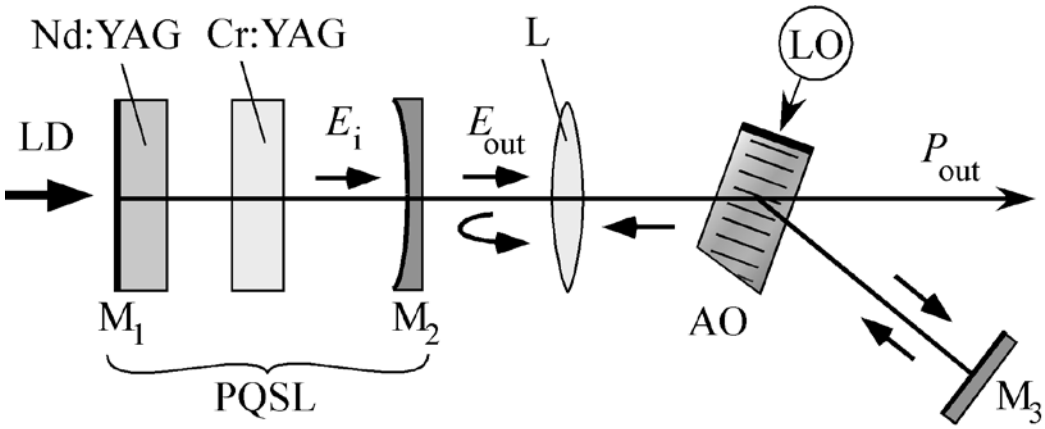
Nd:YAG
Cr:YAG
L
LO
LD
E_i
E_{out}
P_{out}
M_1
M_2
AO
M_3
PQSL

Fig. 1

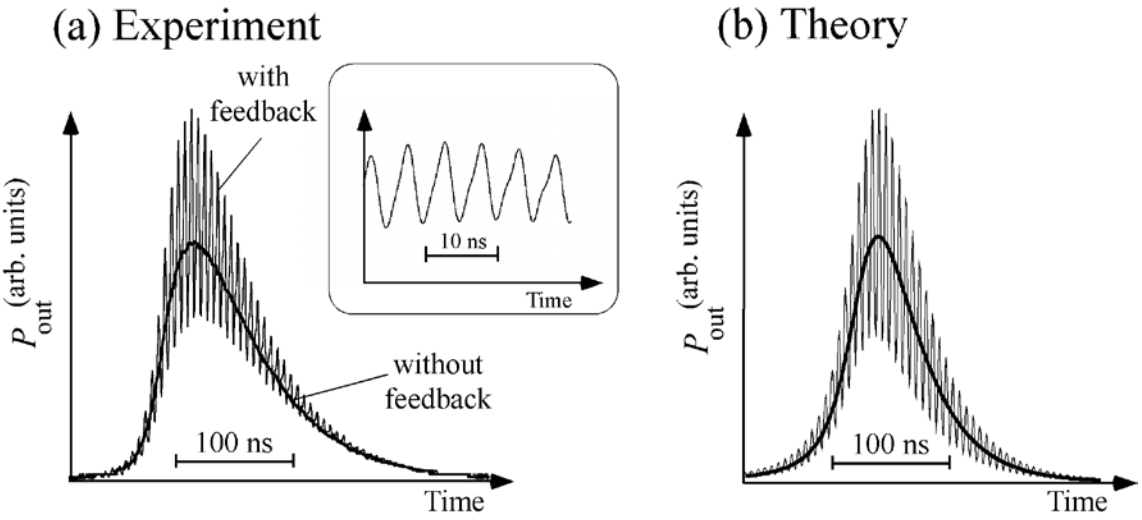
(a) Experiment
(b) Theory
with feedback
without feedback
10 ns
Time
P_{out} (arb. units)
100 ns
Time
P_{out} (arb. units)
100 ns
Time

Fig. 2

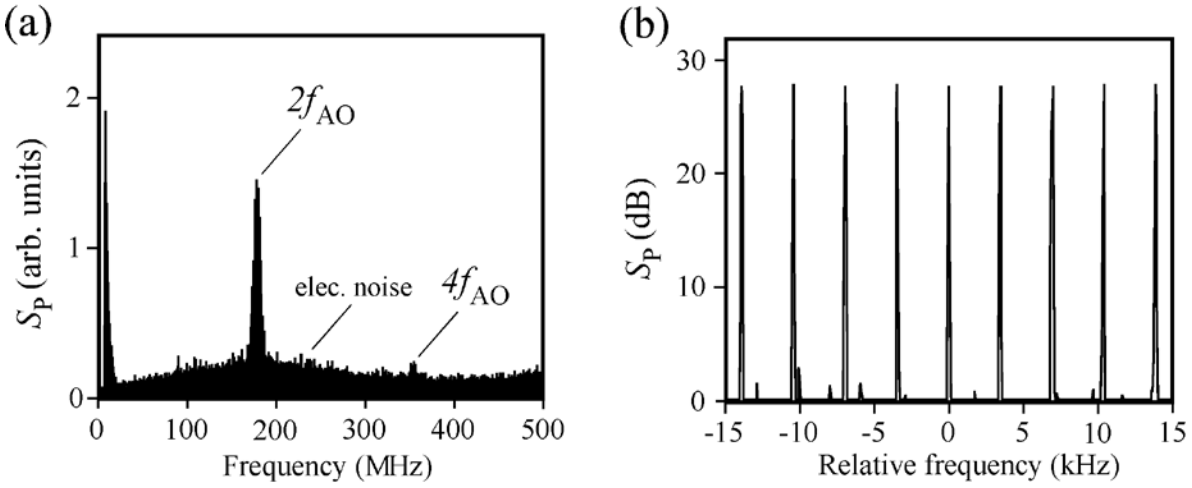
(a)
$2f_{AO}$
elec. noise
$4f_{AO}$
S_P (arb. units)
Frequency (MHz)
(b)
S_P (dB)
Relative frequency (kHz)

Fig. 3

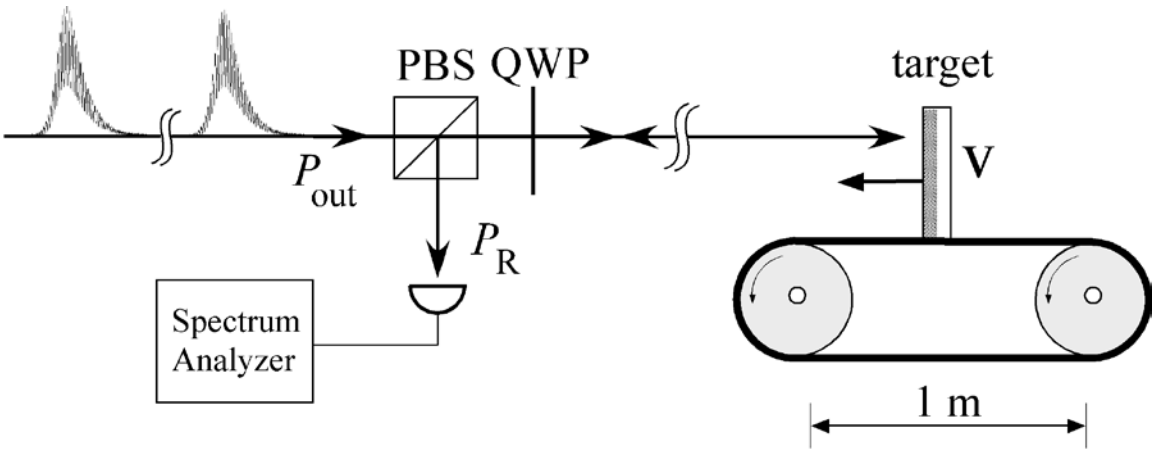
PBS QWP
target
V
P_{out}
P_R
Spectrum Analyzer
1 m

Fig. 4

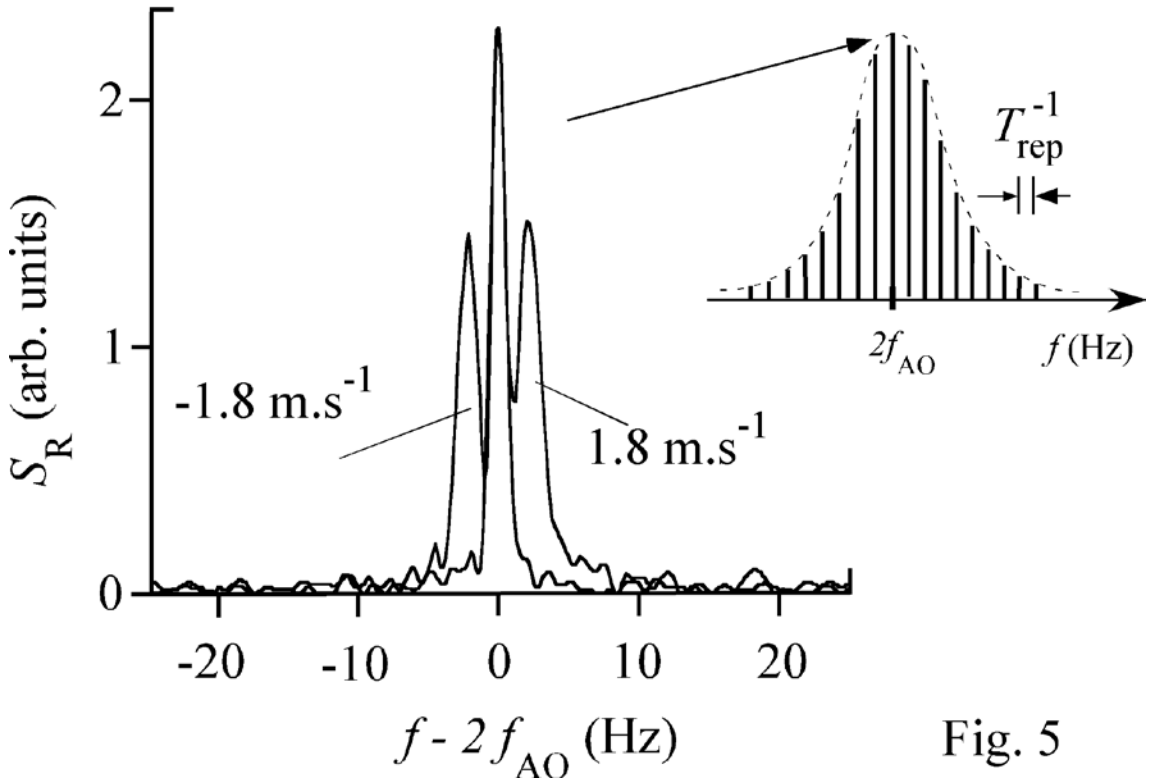
2
1
0
S_R (arb. units)
-1.8 m.s^{-1}
1.8 m.s^{-1}
-20
-10
0
10
20
f - 2f_{AO} (Hz)
T_{rep}^{-1}
2f_{AO}
f (Hz)

Fig. 5

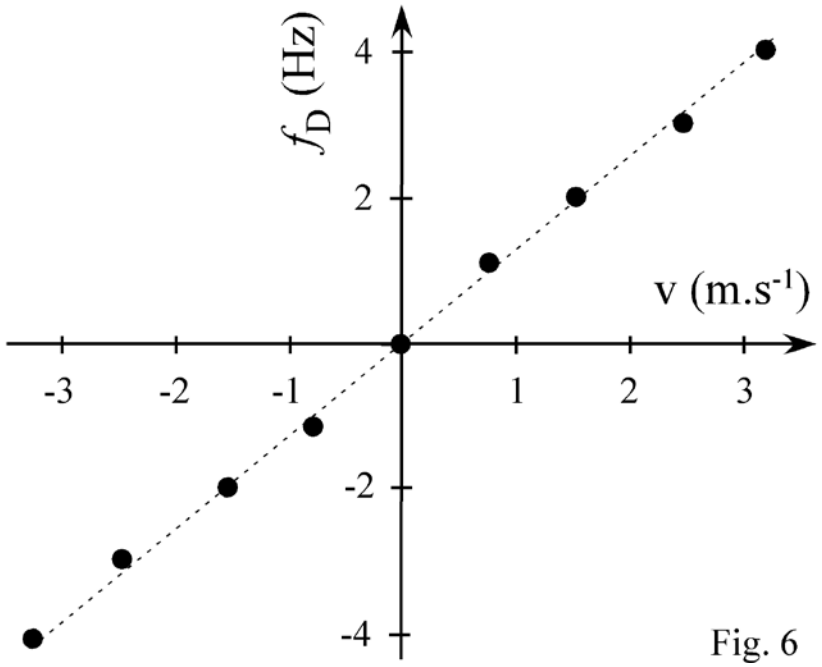
f_D (Hz)
4
2
-2
-4
v (m.s^{-1})
-3
-2
-1
1
2
3

Fig. 6

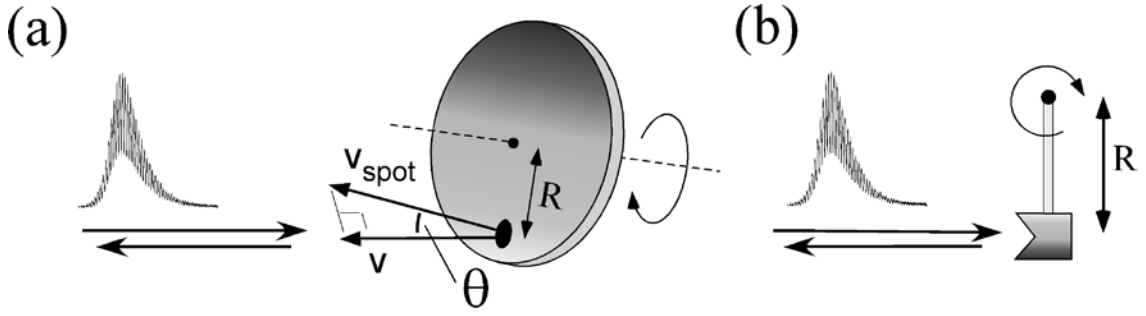
(a)
(b)
v_spot
R
l
v
θ
R

Fig. 7

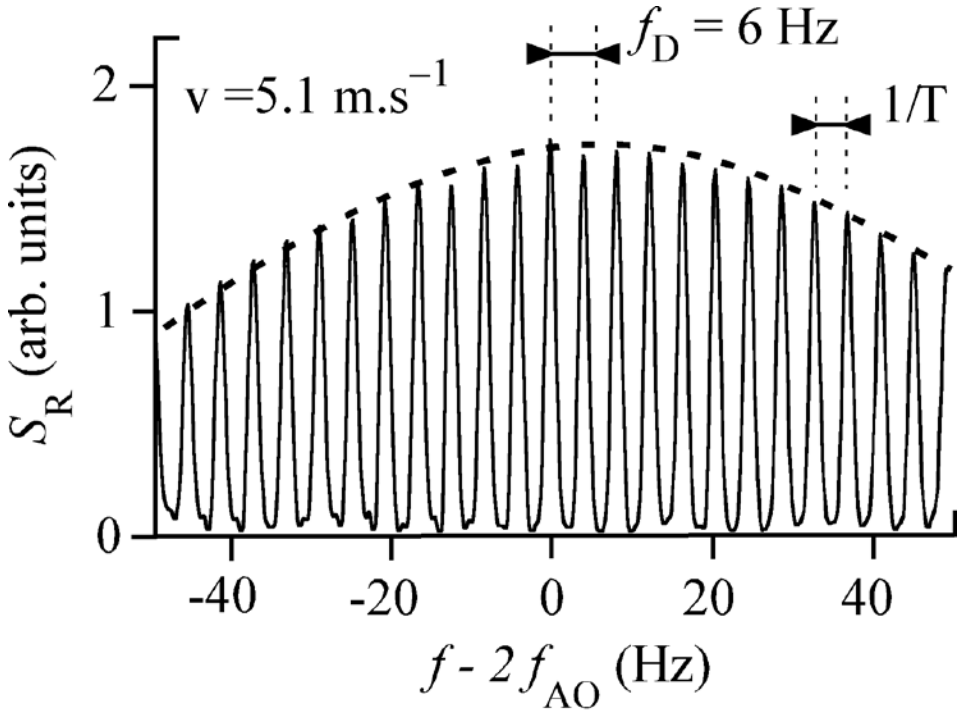
f_D = 6 Hz
v =5.1 m.s^-1
1/T
2
1
0
S_R (arb. units)
-40
-20
0
20
40
f - 2 f_AO (Hz)

Fig. 8

REFERENCES

[1] W. L. Eberhard and R. M. Schotland, “Dual-frequency Doppler-lidar method of wind measurement”, Appl. Opt. **19**, 2967-2976 (1980).

[2] L. J. Mullen, A. J. C. Vieira, P. R. Herczfeld, and V. M. Contarino, “Application of RADAR technology to Aerial LIDAR systems for enhancement of shallow underwater target detection”, IEEE Trans. Microwave Theory Technol. **44**, 2370-2376 (1995).

[3] F. Pellen, P. Olivard, Y. Guern, J. Cariou, and J. Lotrian, “Radio frequency modulation on an optical carrier for target detection enhancement in sea-water”, J. Phys. D: Appl. Phys. **34**, 1122-1130 (2001).

[4] L. De Dominicis, M. Ferri de Collibus, G. Fornetti, M. Guarneri, M. Nuvoli, R. Ricci, and M. Francucci, “Improving underwater imaging in an amplitude modulated laser system with radio frequency control technique”, J. Eur. Opt. Soc. Rapid Pub. **5**, 10004 (2010).

[5] L. Morvan, N. D. Lai, D. Dolfi, J.-P. Huignard, M. Brunel, F. Bretenaker, and A. Le Floch, “Building blocks for a two-frequency laser lidar-radar: a preliminary study”, Appl. Opt. **41**, 5702-5712 (2002).

[6] R. Diaz, S. C. Chan, and J. M. Liu, “Lidar detection using a dual frequency source”, Opt. Lett., **31**, 3600-3602 (2006).

[7] D. C. Kao, T. J. Kane, and L. J. Mullen, “Development of an amplitude-modulated Nd:YAG pulsed laser with modulation frequency tunability up to 60 GHz by dual seed injection”, Opt. Lett. **29**, 1203-1205 (2004).

[8] M. Alouini, B. Benazet, M. Vallet, M. Brunel, P. Di Bin, F. Bretenaker, A. Le Floch, and Ph. Thony, ”Offset phase locking of Er:Yb:glass laser eigenstates for RF photonics applications”, IEEE Photon. Technol. Lett. **13**, 367-369 (2001).

[9] G. Pillet, L. Morvan, D. Dolfi, and J.-P. Huignard, "Wideband dual-frequency Lidar-Radar for high resolution ranging, profilometry and Doppler Measurement", Proc. SPIE **7114**, 71140E (2008).

[10] M. Brunel and M. Vallet, "Pulse-to-pulse coherent beat note generated by a passively *Q*-switched two-frequency laser", Opt. Lett. **33**, 2524-2526 (2008).

[11] A. E. Siegman, *Lasers* (University Science Books, 1986).

[12] N. D. Lai, M. Brunel, F. Bretenaker, and O. Emile, "Control of the pulse duration in one- and two-axis passively *Q*-switched solid-state lasers", Eur. Phys. J. D. **19**, 403-410 (2002).

[13] K. Otsuka, "Ultrahigh sensitivity laser Doppler velocimetry with a microchip solid-state laser", Appl. Opt. **33**, 1111-1114 (1994).

[14] R. Kliese and A. D. Rakić, "Spectral broadening cause by dynamic speckle in self-mixing velocity sensors", Opt. Express **20**, 18757-18771 (2012).

[15] G. Pillet, L. Morvan, D. Dolfi, and J.-P. Huignard, "Wideband dual-frequency Lidar-Radar for simultaneous velocity and high-resolution range profile measurements", Proc. SPIE **7323**, 73230Z (2009).

[16] V. C. Chen, F. Li, S.-S. Ho, and H. Wechsler, "Analysis of micro-Doppler signatures", IEE Proc.-Radar Sonar Navig. **150**, 271-276 (2003).

[17] F. Pellen, V. Jezequel, G. Zion, and B. Le Jeune, "Detection of an underwater target through modulated lidar experiments at grazing incidence in a deep wave basin", Appl. Opt. **51**, 7690-7700 (2012).

[18] Y. Bai, D. Ren, W. Zhao, Y. Qu, L. Qian, and Z. Chen, "Heterodyne Doppler velocity measurement of moving targets by mode-locked pulse laser", Opt. Express **20**, 764-768 (2011).

[19] S. Kameyama, T. Ando, K. Asaka, Y. Hirano, and S. Wadaka, “Compact all-fiber pulsed coherent Doppler Lidar system for wind sensing”, Appl. Opt. **46**, 1953-1962 (2007).